

Supporting Information

Framework-mediated Synthesis of Highly Microporous Onion-like Carbon: Energy Enhancement in Supercapacitors without Compromising Power

*Mahdokht Shaibani,^{ab} Stefan J. D. Smith,^{bc} Parama Chakraborty Banerjee,^a Kristina Konstas,^b Ahmad Zafari,^d Derrek E. Lobo,^a Marziyeh Nazari,^{be} Anthony F. Hollenkamp,^{*b} Matthew R. Hill^{*bc} and Mainak Majumder^{*a}*

Table of contents

Section SI. Supporting Figures

- Figure S1** HRTEM images of MOLC
- Figure S2** EDX elemental analysis and carbonisation yield
- Figure S3** TGA profile of MOLC under atmosphere.
- Figure S4** BET surface area and PSD at 1000 °C
- Figure S5** Cyclic voltammetry of MOLC in different electrolytes at several scan rates
- Figure S6** Capacitance retention ratio as a function of scan rate
- Figure S7** Cyclic voltammetry of PAF-700, PAF-800 and PAF-900 (MOLC)
- Figure S8** Proposed electrical equivalent circuit (EEC)
- Figure S9** Comparison of the simulated data with the experimentally obtained impedance data
- Figure S10** Pore resistance of the MOLC electrodes in various electrolytes

Section SII. Supporting Tables

- Table S1** Texture properties of carbonized samples at different temperatures
- Table S2** Approximate hydrated cation size in three aqueous electrolytes
- Table S3** Capacitances of several nanoporous carbons
- Table S4** Capacitances of several carbon onion based electrodes
- Table S5** Rate capability of MOLC electrodes in various electrolytes
- Table S6** ESR and phase angle of the MOLC electrodes in presence of various electrolytes
- Table S7** Specific capacitance and iR drop values of the MOLC electrode
- Table S8** Areal capacitances of several supercapacitor electrodes

Section SI. Supporting Figures

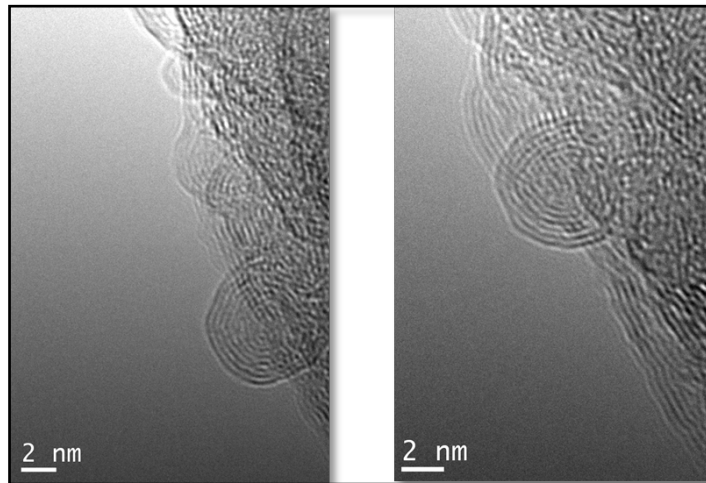


Figure S1 HRTEM images of MOLC.

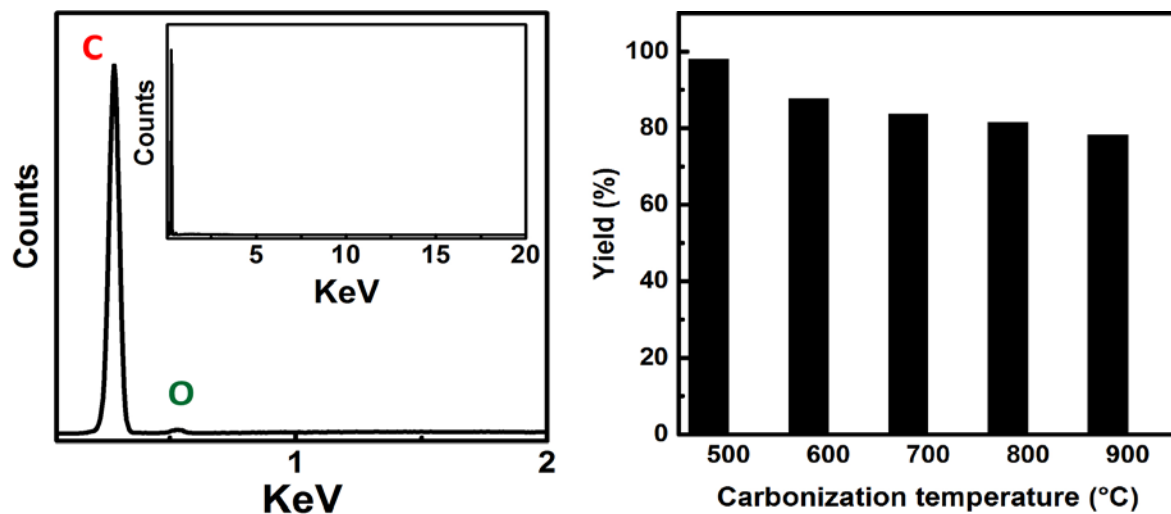


Figure S2(a) EDX elemental analysis showing the high purity of the PAF derived carbon; (b) Carbonisation yield of directly carbonized PAF-1 at various temperatures. It is noteworthy that the conversion yield of diamondoid PAF-1 to carbon is considerably high compared to the literature.^[2] A high yield in conversion means that less of a well-structured porous material has to be synthesized, treated and loaded in the carbonisation unit and most importantly less fuel is burned. We attribute the high conversion efficiency of PAF-1 to two major factors: a) the high carbon content of the template b) absence of any pre/post treatments.

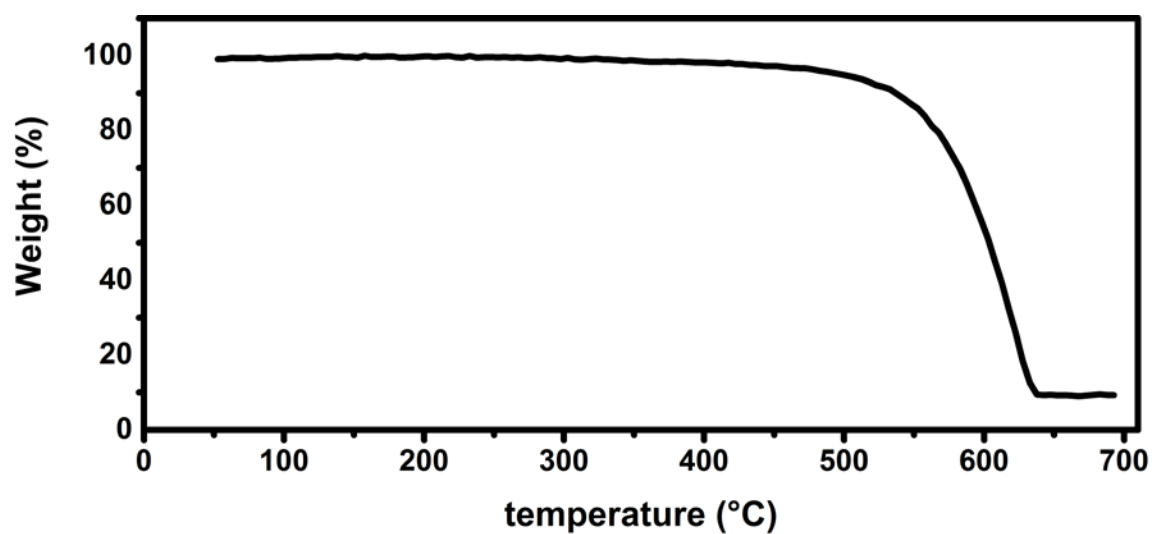


Figure S3 The TGA profile of MOLC under atmosphere.

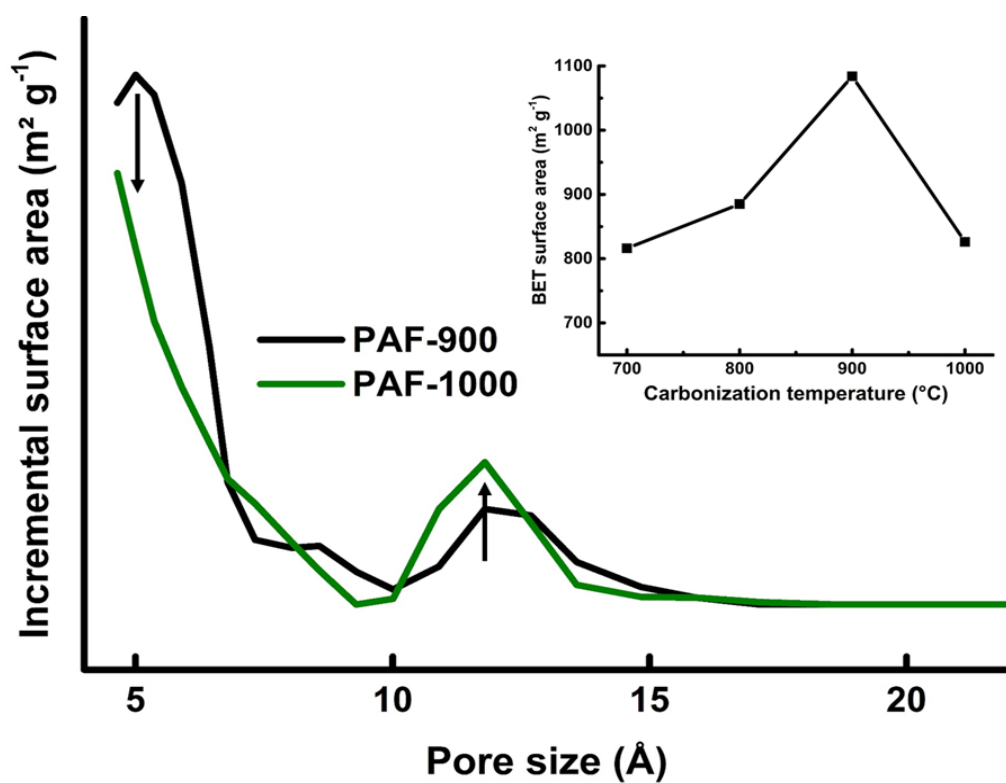


Figure S4 Effect of high temperature carbonization on surface area and pore size distribution of the resultant carbon.

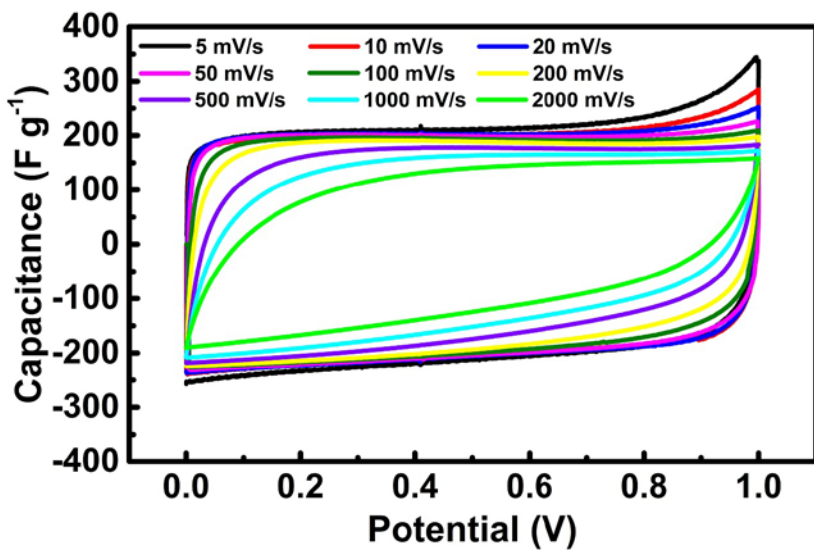
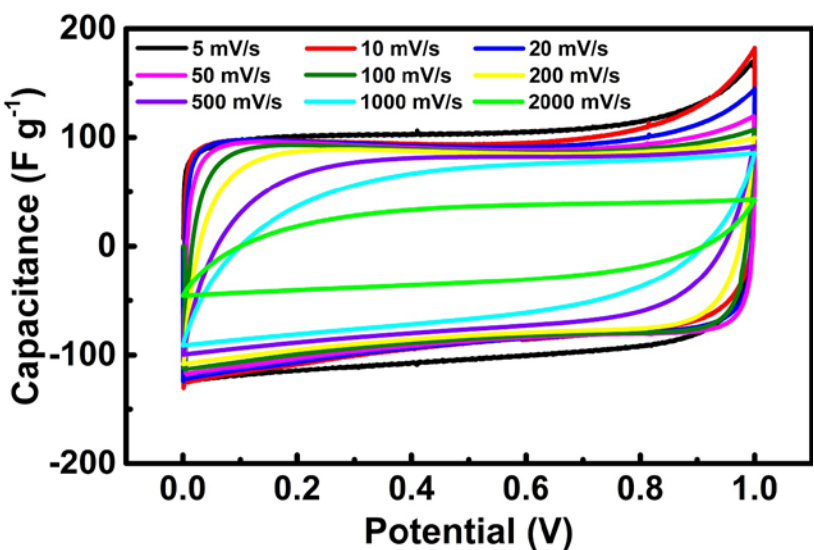
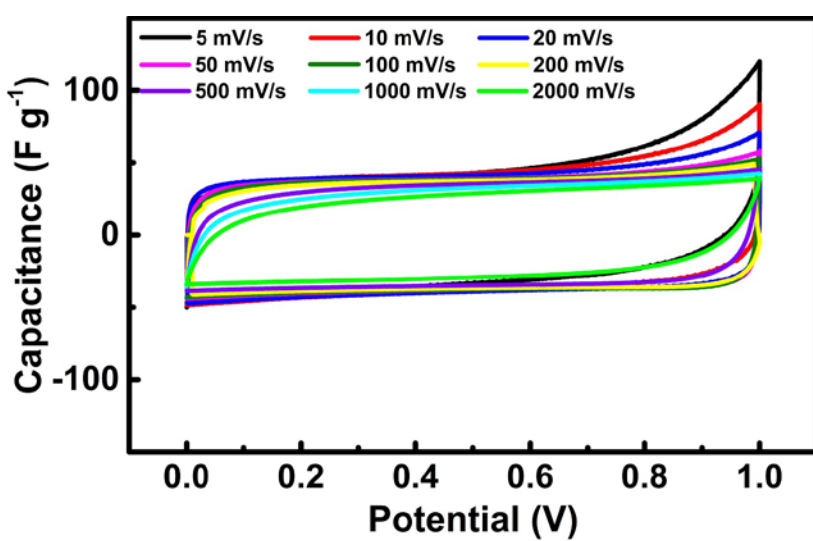
a**b****c**

Figure S5 Cyclic voltammetry of MOLC over a potential range of 0-1 V in a) KOH, b) NaOH, c) LiOH at several scan rates.

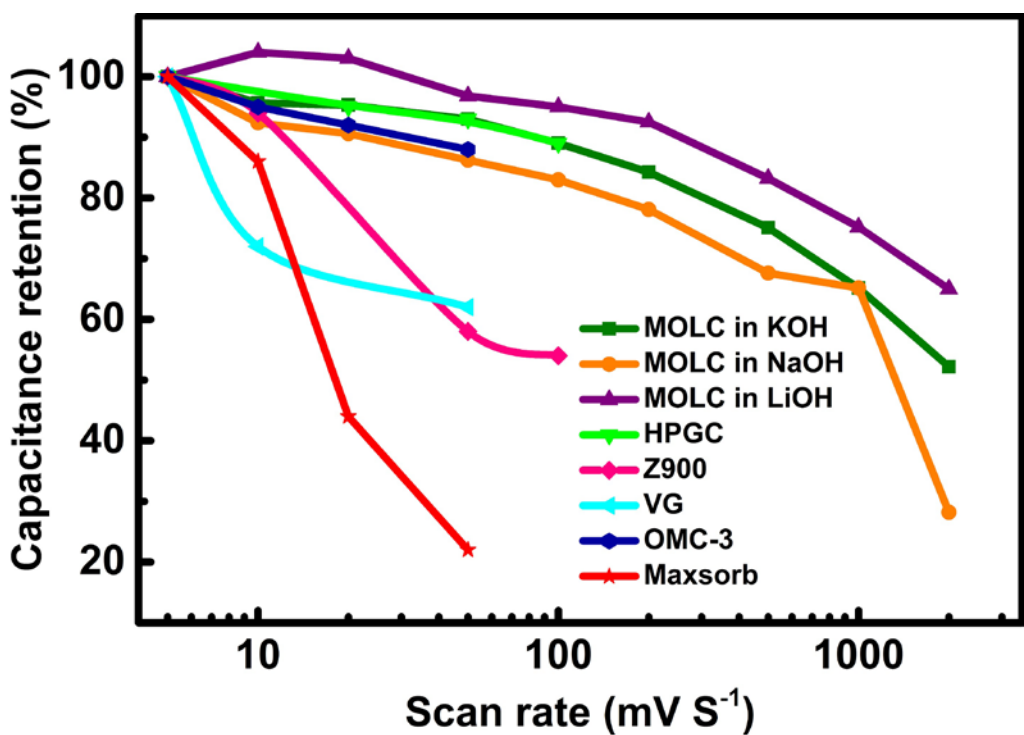


Figure S6 Capacitance retention ratio as a function of scan rate for MOLC in three alkaline electrolyte and also other advanced carbon materials cycled in similar conditions, i. e. two electrode devices, ~ 1V potential window and aqueous electrolyte: HPGC, hierarchical porous graphitic carbon^[1]; Z950, ZIF-8 derived carbon^[3]; VG, vertically-oriented graphene^[5]; OMC, ordered mesoporous carbon^[7] and Maxsorb^[1, 7], commercially used activated carbon. Cycling MOLC in LiOH demonstrates the highest rate capability amongst the three alkaline based electrolytes as the contribution of pores in the formation of double layer is relatively low and independent of the scan rate.

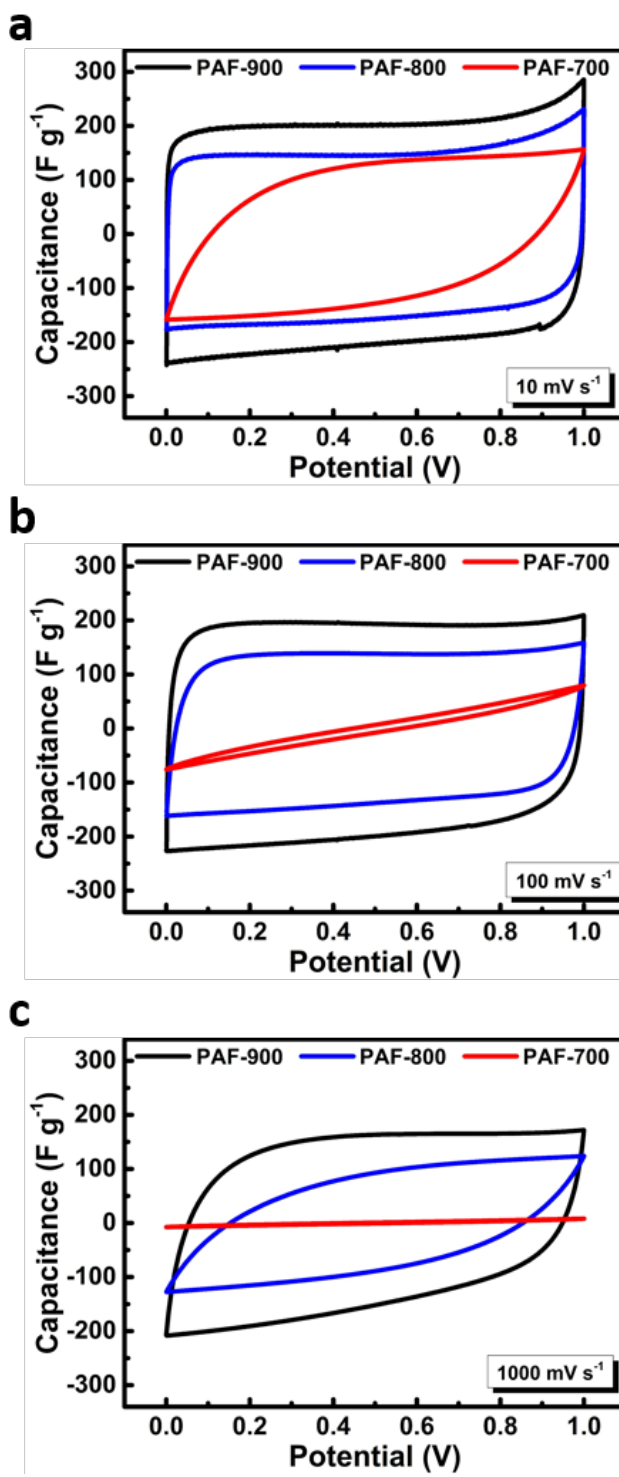


Figure S7 Cyclic voltammetry of PAF-700, PAF-800 and PAF-900 (MOLC) over a potential range of 0-1 V in KOH electrolyte at different scan rates.

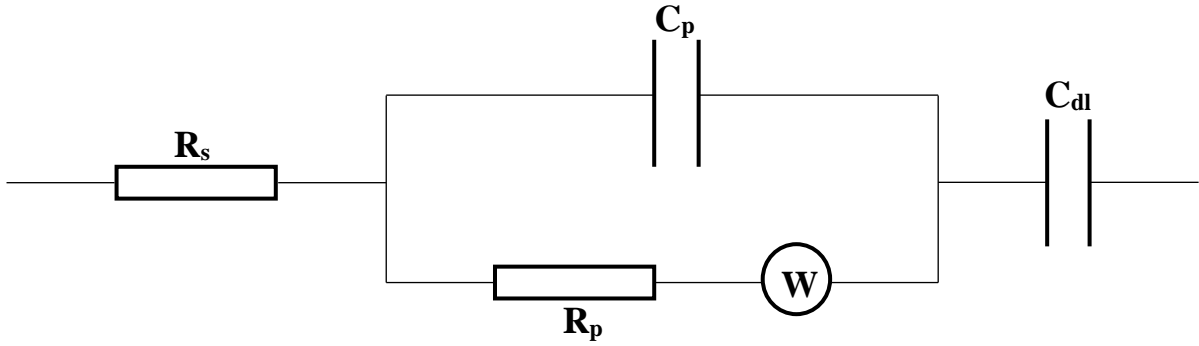


Figure S8 Proposed electrical equivalent circuit (EEC) to analyse the impedance data of the MOLC electrodes in various electrolytes. The EEC consists of a series combination of an electrolyte resistance (R_s), a time constant, representing the electrolyte diffusion kinetics through the pores, and a double layer capacitance (C_{dl}), representing the capacitance arising due to the adsorption/desorption of the electrolyte at the outer surfaces of the carbon onions. The time constant consists of a pore capacitance (C_p) connected in parallel with a series combination of a pore resistance (R_p) and a Warburg element (W) related to the diffusion of the hydrated ions through the pores.

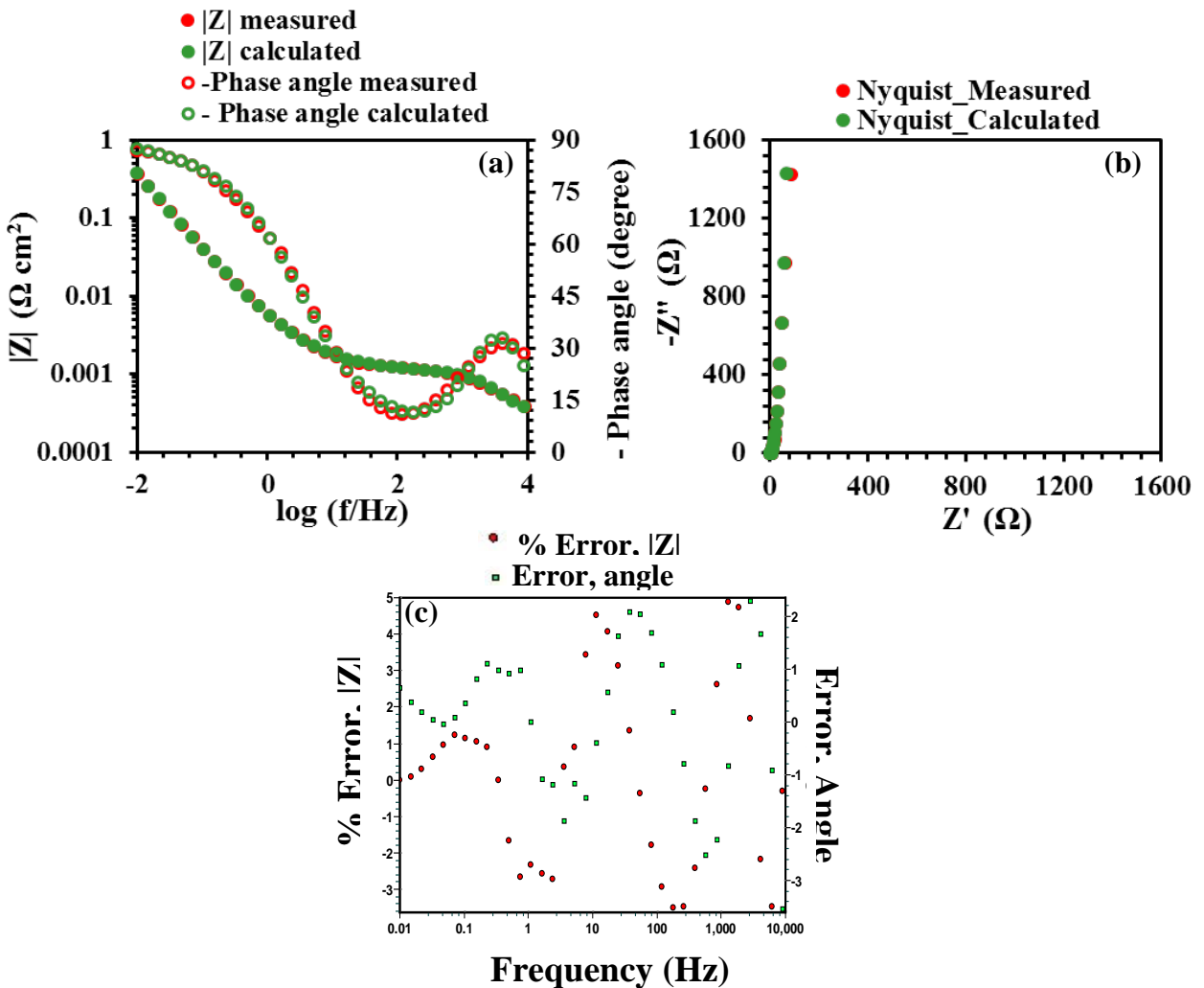


Figure S9 A comparison of the simulated data with the experimentally obtained impedance data; (a) Bode and (c) Nyquist plots in case of the MOLC electrodes in presence of KOH. (c) Representative error plots for the experimental and simulated impedance data. The error plot indicates that the total error in $|Z|$ was less 6% and the total error in angle was less than 4 degree. The low total error in $|Z|$ and angle confirms the validity of the proposed EEC in explaining the experimental impedance data.

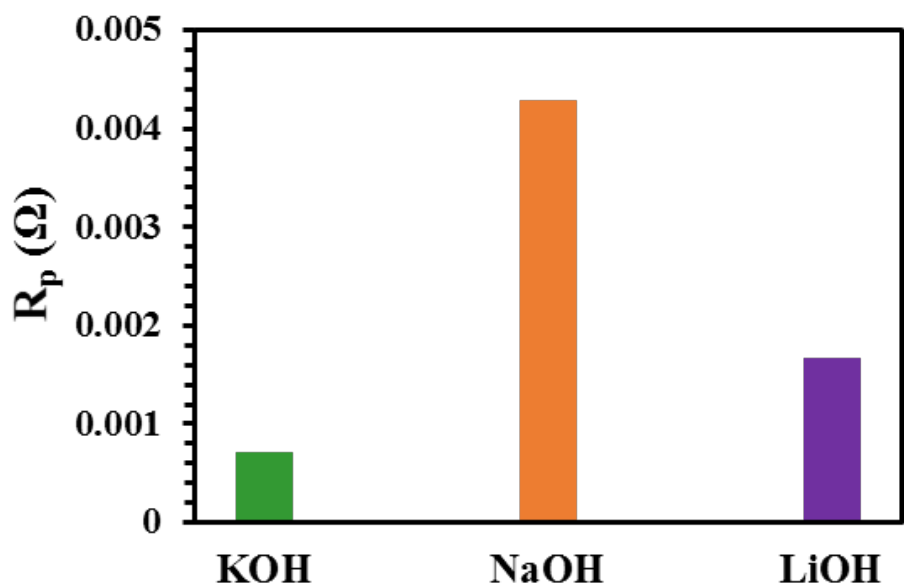


Figure S10 Pore resistance (R_p) of the MOLC electrodes in presence of KOH, NaOH and LiOH.

Section SII. Supporting Tables

Table S1 Texture properties of carbonized samples at different temperatures.

Material	BET SSA (m ² g ⁻¹)	External Surface area	Microporous Surface area	Pore size distribution (Å)
PAF-700	816	135	681	≈5, ≈11.8
PAF-800	885	159	726	≈5, ≈11.8
PAF-900	1084	217	867	≈5, ≈11.8

Table S2 Approximate hydrated cation size in three aqueous electrolytes used in this work and the fraction of pores in PAF-900 which could accommodate each from a simple geometric consideration.

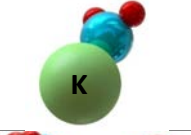
Electrolyte	Hydrated cation	Schematic representation	Hydrated cation size (Å)	~Fraction of available pores (%)
KOH	K ⁺ (aq)		4.64	100
NaOH	Na ⁺ (aq)		5.52	50
LiOH	Li ⁺ (aq)		6.80	22

Table S3 Capacitances of several nanoporous carbons with BET SSA higher or close to MOLC in this work. It is seen that a high surface area and a large pore volume are not necessarily required for a large capacitance.

Carbon material	BET SSA $\text{m}^2 \text{ g}^{-1}$	Capacitance F g^{-1}
C1000^[10]	3405	161 @ 5 mV s ⁻¹
C800^[10]	2169	188 @ 5 mV s ⁻¹
NPC^[11]	2872	204 @ 5 mV s ⁻¹
Z900^[12]	1075	214 @ 5 mV s ⁻¹
NPC1000^[13]	2542	120 @ 5 mV s ⁻¹
AS-ZC-800^[14]	2972	211 @ 10 mV s ⁻¹
Maxsorb^[7]	3310	289 @ 10 mV s ⁻¹
OMC-3^[7]	1703	196 @ 10 mV s ⁻¹
HP-CNS^[15]	1946	121 @ 0.5 A g ⁻¹
IMPC^[16]	1327	255 @ 0.5 A g ⁻¹

Table S4 Capacitances of several carbon onion based electrodes.

Carbon material	BET SSA $\text{m}^2 \text{ g}^{-1}$	Capacitance F g^{-1}
CNOs(1650)-N2^[4]	385	35.5 @ 20 mV s ⁻¹
OLC (1750)- vacuum^[6]	391	12 @ 2 mV s ⁻¹
1700-AR^[8]	430	24 @ 1 A g ⁻¹
ND 1200^[9]	500	30 @ 0.2 A cm ⁻²
ND 2000^[9]	460	20 @ 0.2 A cm ⁻²

Table S5 Percentage decrease in the specific capacitance of the MOLC electrodes in various electrolytes as a function of the scan rate.

Scan rate (mV s ⁻¹)	Percentage decrease in specific capacitance (%)		
	KOH	NaOH	LiOH
10	4.3	7.6	0
20	4.7	9.4	0
50	7.2	13.7	3.2
100	11.2	17.0	5.0
200	15.7	21.9	7.5
500	24.9	32.3	16.8
1000	34.8	34.8	24.8
2000	47.8	71.8	35.0

Table S6 ESR and phase angle of the MOLC electrodes in presence of various electrolytes. The resistances are normalised per unit gram of electrode material.

Condition	ESR (mΩ)	Phase angle (degree)
KOH	0.2	-86.7
NaOH	0.6	-85.5
LiOH	0.3	-84

Table S7 Specific capacitance and iR drop values of the MOLC electrodes.

Current density (A g ⁻¹)	KOH		NaOH		LiOH	
	iR drop (V)	Capacitance (F g ⁻¹)	iR drop (V)	Capacitance (F g ⁻¹)	iR drop (V)	Capacitance (F g ⁻¹)
0.5	0.002	202	0.015	80	0.004	38
1	0.007	192	0.03	75	0.01	35
2	0.013	186	0.06	68	0.018	34

Table S8 Areal capacitances of several supercapacitor electrodes

Electrode material	Areal density (mg cm ⁻²)	Areal capacitance (F cm ⁻²)
NiCo ₂ O ₄ ^[17]	0.9	3.12 @ 1.11 mA cm ⁻² 1.44 @ 2.78 mA cm ⁻² 1.01 @ 5.56 mA cm ⁻² 0.79 @ 11.12 mA cm ⁻² 0.59 @ 22.24 mA cm ⁻²
Carbon nanofiber ^[18]	60	1.2 @ 1 mA cm ⁻²
GF/CNT/MnO ₂ hybrid films ^[19]	6.2	0.78 @ 5 mV s ⁻¹ 0.50 @ 10 mV s ⁻¹ 0.30 @ 20 mV s ⁻¹ 0.15 @ 50 mV s ⁻¹
CP-1200 (PEDOT) ^[20]	7.56	0.836 @ 0.5 A g ⁻¹
2D Titanium carbide ^[21]	7.6	0.579 @ 2 mV s ⁻¹
Ni@NiO core-shell electrode ^[22]	-	2.04 @ 8 mA cm ⁻² 1.13 @ 20 mA cm ⁻²
3D Graphene Hydrogel Films ^[23]	2	0.372 @ 1 A g ⁻¹
Graphene-Polypyrrole Hybrid paper ^[24]	2.7	0.44 @ 0.5 A g ⁻¹ 0.30 @ 6 A g ⁻¹
Hierarchical carbon tubular nanostructures ^[25]	1.3	0.321 @ 5 mV s ⁻¹ 0.066 @ 10 mV s ⁻¹ 0.044 @ 20 mV s ⁻¹
Lignin-derived interconnected hierarchical porous carbon ^[26]	14.4	3.0 @ 0.1 A g ⁻¹ 1.4 @ 10 A g ⁻¹
3D MnO ₂ –graphene composite ^[27]	13.6	3.18 @ 1 mV s ⁻¹
This work	≈8	3.03 @ 0.25 A g ⁻¹ 3.0 @ 0.5 A g ⁻¹ 2.94 @ 1 A g ⁻¹ 2.87 @ 2 A g ⁻¹

References

- [1] D. W. Wang, F. Li, M. Liu, G. Q. Lu, H. M. Cheng, *Angew. Chem.* 2008, 120, 379.
- [2] Y. Li, S. Roy, T. Ben, S. Xu, S. Qiu, *PCCP* 2014, 16, 12909; Y. Li, T. Ben, B. Zhang, Y. Fu, S. Qiu, *Scientific reports* 2013, 3.
- [3] P. Zhang, F. Sun, Z. Shen, D. Cao, *Journal of Materials Chemistry A* 2014.
- [4] O. Mykhailiv, A. Lapinski, A. Molina - Ontoria, E. Regulska, L. Echegoyen, A. T. Dubis, M. E. Plonska - Brzezinska, *ChemPhysChem* 2015.
- [5] Z. Bo, Z. Wen, H. Kim, G. Lu, K. Yu, J. Chen, *Carbon* 2012, 50, 4379.
- [6] K. Makgopa, P. M. Ejikeme, C. J. Jafta, K. Raju, M. Zeiger, V. Presser, K. I. Ozoemena, *Journal of Materials Chemistry A* 2015, 3, 3480.
- [7] W. Xing, S. Z. Qiao, R. G. Ding, F. Li, G. Q. Lu, Z. F. Yan, H. M. Cheng, *Carbon* 2006, 44, 216.
- [8] M. Zeiger, N. Jäckel, D. Weingarth, V. Presser, *Carbon* 2015, 94, 507.
- [9] C. Portet, G. Yushin, Y. Gogotsi, *Carbon* 2007, 45, 2511.
- [10] H.-L. Jiang, B. Liu, Y.-Q. Lan, K. Kuratani, T. Akita, H. Shioyama, F. Zong, Q. Xu, *J. Am. Chem. Soc.* 2011, 133, 11854.
- [11] B. Liu, H. Shioyama, T. Akita, Q. Xu, *J. Am. Chem. Soc.* 2008, 130, 5390.
- [12] W. Chaikittisilp, M. Hu, H. Wang, H.-S. Huang, T. Fujita, K. C.-W. Wu, L.-C. Chen, Y. Yamauchi, K. Ariga, *Chem. Commun.* 2012, 48, 7259.
- [13] B. Liu, H. Shioyama, H. Jiang, X. Zhang, Q. Xu, *Carbon* 2010, 48, 456.
- [14] A. J. Amali, J.-K. Sun, Q. Xu, *Chem. Commun.* 2014, 50, 1519.
- [15] Y. S. Yun, M. H. Park, S. J. Hong, M. E. Lee, Y. W. Park, H.-J. Jin, *ACS Applied Materials & Interfaces* 2015.
- [16] D. Puthusseri, V. Aravindan, S. Madhavi, S. Ogale, *Energy & Environmental Science* 2014, 7, 728.
- [17] G. Q. Zhang, H. B. Wu, H. E. Hostler, M. B. Chan-Park, X. W. D. Lou, *Energy & Environmental Science* 2012, 5, 9453.
- [18] J. R. McDonough, J. W. Choi, Y. Yang, F. La Mantia, Y. Zhang, Y. Cui, *Appl. Phys. Lett.* 2009, 95, 243109.
- [19] J. Liu, L. Zhang, H. B. Wu, J. Lin, Z. Shen, X. W. D. Lou, *Energy & Environmental Science* 2014, 7, 3709.
- [20] B. Anothumakkool, S. N. Bhange, M. V. Badiger, S. Kurungot, *Nanoscale* 2014, 6, 5944.
- [21] S.-Y. Lin, X. Zhang, *J. Power Sources* 2015, 294, 354.
- [22] M. Yu, W. Wang, C. Li, T. Zhai, X. Lu, Y. Tong, *NPG Asia Materials* 2014, 6, e129.
- [23] Y. Xu, Z. Lin, X. Huang, Y. Liu, Y. Huang, X. Duan, *ACS nano* 2013, 7, 4042.
- [24] K. Shu, C. Wang, C. Zhao, Y. Ge, G. G. Wallace, *Electrochim. Acta* 2016, 212, 561.
- [25] H. Zhang, H. Su, L. Zhang, B. Zhang, F. Chun, X. Chu, W. He, W. Yang, *J. Power Sources* 2016, 331, 332.
- [26] H. Li, D. Yuan, C. Tang, S. Wang, J. Sun, Z. Li, T. Tang, F. Wang, H. Gong, C. He, *Carbon* 2016, 100, 151.
- [27] T. Zhai, F. Wang, M. Yu, S. Xie, C. Liang, C. Li, F. Xiao, R. Tang, Q. Wu, X. Lu, *Nanoscale* 2013, 5, 6790.